Visualisation of calculated thermodynamic properties by integration of FactSage with SEM-EDS element maps

N. Barrett[1], S. Mitra[2], E. Copland[3], D. O'Dea[4] and T. Honeyands[5]

1.Research Associate, Centre for Ironmaking Materials Research, Newcastle NSW 2307. Email: Nathan.barrett@newcastle.edu.au
2.Research Associate, Centre for Ironmaking Materials Research, Newcastle NSW 2307. Email: Subhasish.mitra@newcastle.edu.au
3. Research Associate, Centre for Ironmaking Materials Research, Newcastle NSW 2307. Email: Evan.copland@newcastle.edu.au
4. Principal Sustainability Marketing, BHP, Brisbane QLD 4000. Email: Damien.p.odea@bhp.com
5. Co-Director, Centre for Ironmaking Materials Research, Newcastle NSW 2307. Email: Tom.a.honeyands@newcastle.edu.au

Keywords: Thermodynamics, EDS, Mapping, Blast Furnace, Interaction

ABSTRACT

This work describes a novel mapping technique that allows the direct overlay of calculated local phase equilibria on micrographs of the physical system. The technique demonstrated integrates FactSage phase equilibria calculations with mapped compositions determined by SEM-EDS to visually express calculated properties while preserving the spatial information of the sample. The developed methodology is used to analyse interrupted blast furnace softening and melting tests containing mixed burdens of lump and sinter. Tests are interrupted at 1300 °C and cooled to room temperature for analysis. Phases present at room temperature are analysed to infer the liquid fraction and phases present at high temperature. Analysis of the interface regions between the dissimilar burdens allows insights to be gained into the interaction mechanism. During the transition from solid to liquid, migration and interaction of liquid oxide across the interfaces of the dissimilar burdens has been observed and demonstrated to impact softening and melting performance. Specifically, interaction of the oxides generated by lump (primarily FeO, SiO_2 and Al_2O_3) and sinter (primarily FeO, CaO, SiO_2, Al_2O_3 and MgO) are analysed, and the occurrence of a range of new mineral phases such as merwinite, melilite, olivine and bredigite observed.

INTRODUCTION

The ironmaking blast furnace currently provides ~72% of the hot metal for steelmaking globally, the total production of which exceeded 1.8 billion tonnes in 2023 (World Steel Association, 2023). While many blast furnaces operate with predominantly sinter (iron ore fines agglomerated with fluxes), supplementation with lump ore (natural iron ore of an appropriate size for direct charging) is beneficial, as it avoids emissions associated sinter production (Liu, Honeyands, Evans, O'Dea, & Ellis, 2018; Liu, Honeyands, O'Dea, Chen, & Qiu, 2019). The natural gangue in lump ores is primarily SiO_2 and Al_2O_3, while sinter contains added CaO and MgO flux. As such, with the differing chemical composition of the two burdens, chemical interactions occur at high temperatures during softening and melting. These interactions have been demonstrated to be beneficial to cohesive zone performance, improving the permeability of ferrous burden to rising gas (Hoque et al., 2021; Liu, Honeyands, O'Dea, et al., 2019; Lu, Wu, Du, & Zhou, 2020; Wu, Su, Liu, & Kou, 2018).

During its descent in the furnace stack, ferrous burden is reduced (oxygen is removed), resulting in the formation of metallic iron. From this, the microstructure at the onset of melting is an interconnected metallic iron network partitioned from oxide gangue (Kim et al., 2021; Vemdrame Flores, Matos, Lima da Silva, & Covcevich Bagatini, 2021). With the variation in composition at the interface between dissimilar burdens, liquid formation and interaction (>1200 °C) depends on the local composition. As such, it is appropriate that methods of analysis consider the local interfacial compositions, rather than bulk composition.

Thermodynamics is used to describe the chemical processes that occur in extractive metallurgical operations. Of particular importance in the extraction and refining of metals is the properties of the formed slag – which acts to partition impurities from product metal. These slags are typically multicomponent metal oxides. Bulk compositions of slags produced by sinter and lump ore can be plotted on ternary phase diagrams, allowing various thermodynamic variables to be analysed, such as liquidus temperature, stable phase fields, etc. Where more than three components are present (as is the case with most operations), pseudo-ternary diagrams are used, for which additional component compositions are fixed. These diagrams show ‘slices’ through the higher dimensional phase fields, and as such their interpretation can be more difficult. This is especially the case in heterogenous systems, in which the range of compositions present may not be directly expressible in a single diagram.

While elemental mapping techniques (such as SEM-EDS (Hoque et al., 2021; Liu, Honeyands, Evans, Chen, & O’Dea, 2019; Lu et al., 2020; Lyu, Wang, et al., 2023; Lyu, Yang, et al., 2023; Ma et al., 2022; Wu, Han, Xu, Wang, & Liu, 2010) and EPMA (Liu et al., 2018; Liu, Honeyands, O'Dea,

et al., 2019)) have been used historically, thermodynamic analysis has only been performed for compositions determined by bulk chemical analysis (of initial material (Hoque et al., 2021; Liu, Honeyands, Evans, et al., 2019; Liu et al., 2018) or collected slags (Liu, Wu, Huang, Zhang, & Du, 2014; Wang, Diao, Xie, Qi, & Du, 2022; Wu, Lu, Hong, & Zhou, 2020; Wu et al., 2018)) or point analysis (Lyu, Wang, et al., 2023; Wang et al., 2022). From these techniques, the interaction between lump and sinter has been generally described. The interaction is thought to be initiated by low temperature fayalitic (FeO/SiO_2) melts originating from the lump (Liu, Honeyands, O'Dea, et al., 2019; Wang et al., 2022; Wu et al., 2020). On contact with CaO and MgO rich sinter phases, these liquids re-solidify as new phases such as olivine ($CaFeSiO_4$), merwinite ($Ca_3MgSi_2O_8$) and melilite (mainly akerminite ($Ca_2MgSi_2O_7$) and gehlenite($Ca_2Al_2SiO_7$)) (Liu, Honeyands, O'Dea, et al., 2019; Liu et al., 2014).

In this study, a new approach to thermodynamic analysis of real systems is demonstrated through the investigation of an interface between dissimilar ferrous burdens during softening and melting (Barrett et al., 2024). The developed technique integrates element maps (acquired by SEM-EDS) with thermodynamic calculations (performed with FactSage) to directly overlay the calculated phase equilibrium onto the imaged microstructure. The resulting images preserve the spatial composition information, allowing intuitive analysis of phase distribution in a multi-component heterogenous system. The developed technique has potential applications in the pyrometallurgy field far beyond the presented example.

METHODOLOGY

Softening and Melting Test

The Softening and Melting (S&M) test is designed to characterise ferrous burden behaviour in the blast furnace. During the tests, ferrous material is exposed to a temperature profile and reducing gas while under load. As the temperature increases, the material contracts (softens), restricting gas flow, before melting and dropping from the crucible. The bulk performance of the material is characterised through derived indices related to its temperature dependant contraction and pressure drop.

In this study, two ferrous burdens were used, designed around a mixed burden of 20% lump and 80% sinter previously studied (Barrett, Mitra, Chew, O'dea, & Honeyands, 2023; Hoque et al., 2021; Liu, Honeyands, O'Dea, et al., 2019). The lump ore used was Newman Blend Lump, an Australian high-grade hematite-goethite (henceforth referred to as NBLL). The sinter was a high basicity plant sinter (henceforth referred to as SH1). The composition of the burdens are given in Table 1.

TABLE 1 – Chemcial composition of burdens used in this study

Burden	TFe (wt%)	FeO (wt%)	CaO (wt%)	SiO_2 (wt%)	Al_2O_3 (wt%)	MgO (wt%)
NBLL	62.8	-	0.05	3.70	1.4	0.1
SH1	56.7	7.6	10.04	5.43	1.87	1.76

The sample analysed in this study was subject to a standard S&M test, before being interrupted at 1300 °C. Details of the experimental apparatus and conditions can be found elsewhere (Barrett et al., 2023; Hoque et al., 2021). After reaching 1300 °C, the furnace was cooled under 14 L/min nitrogen, reaching 1100 °C within approximately 30 minutes.

Thermodynamic Analysis

In this study, a novel technique for analysis in heterogenous systems was developed, in which calculated phase equilibrium at specific local conditions was directly overlayed on the imaged microstructure. The developed technique is akin to repeated point analysis, for which an equilibrium calculation is performed for every point. An overview of the procedure is described below.

Selection of Interface

Samples from mixed burden S&M tests (reduced under a 70% $N_{2,(g)}$ + 30% $CO_{(g)}$ atmosphere) interrupted at 1300 °C were used, the same as in a previous study (Barrett et al., 2023). The heating profile consisted of 10 °C/min up to 600 °C, followed by a 3.6 °C/min up to 950 °C, 1.9 °C up to 1230 °C and 4.7 °C up to 1300 °C. The resulting reduction degree was approximately 90% (as approximated for the overall burden). The selected interruption temperature was above the temperature of the first formation of liquid slag (~1200 °C), but below the temperature where significant movement and dynamic mixing of the bulk liquid is expected (~1450 °C).

Following the interruption of the test, the crucibles were set in resin, sectioned longitudinally and polished for microscopic analysis. Figure 1 (left) shows the light optical microscopy image of the entire crucible of material. From the lump particles present, an interface contacting sinter was chosen for detailed analysis. A magnified view of the selected region is shown in Figure 1 (right), with the scanned area outlined in red. The phases present on cooling from 1300 °C could then be analysed to infer conditions present at high temperature. It was assumed that no changes to the microstructure occur during cooling.

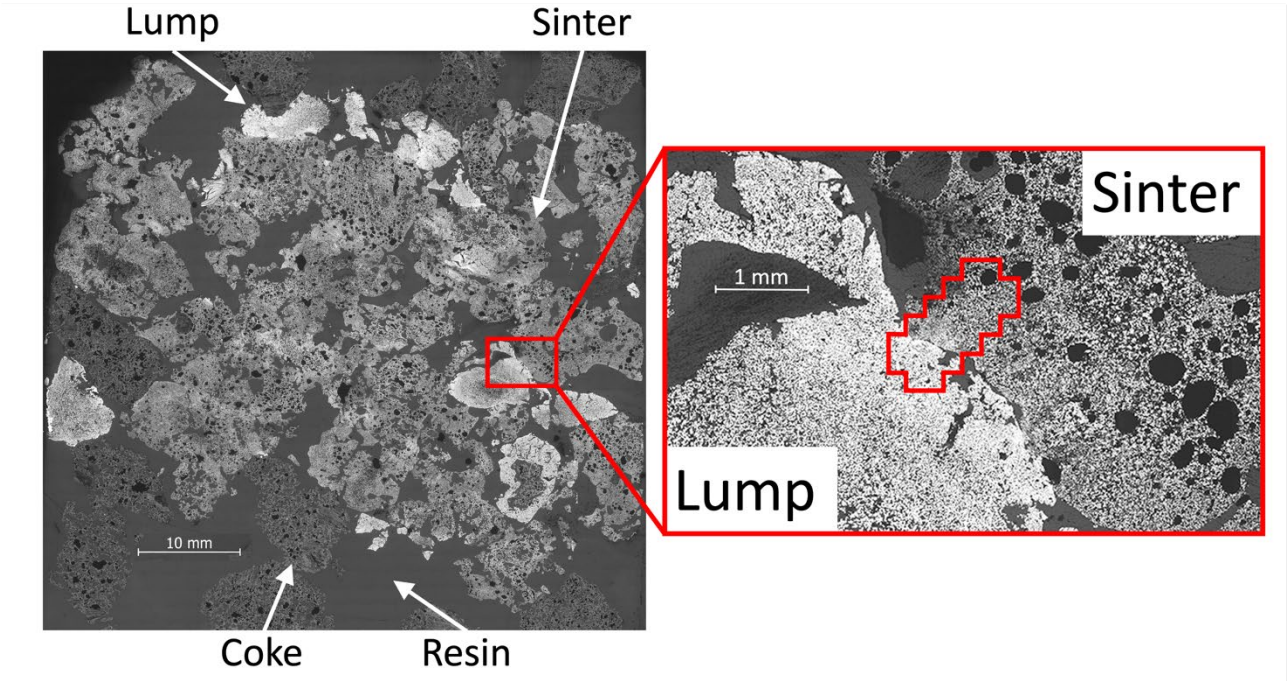

FIG 1 – Light optical microscopy images of sectioned crucible (left) and enlarged interface between lump and sinter (right). Scanned area for detailed analysis is outlined in red.

Data Acquisition (SEM-EDS)

A Tescan Integrated Mineral Analyser (TIMA) was used for SEM-EDS data acquisition. The sample was carbon coated for use in the SEM. The TIMA was equipped with four EDS detectors, facilitating rapid analysis.

The selected scan area highlighted as the red region in Figure 1 (right) was composed of multiple 200 µm fields with a pixel spacing of 4 µm (close to the practical resolution / beam interaction volume). A working distance of 15 mm at an acceleration voltage of 25 keV was used, with 30,000 x-ray counts collected per pixel. Spectra were acquired for all pixels of which the Back Scattered Electron (BSE) intensity was greater than 15%, to avoid scanning areas without material (resin or pores). The BSE image of the acquired scan is shown in Figure 2 (left), with an approximately marked interface between the lump and sinter marked in blue. In Figure 2 (right) an enlarged field is shown, with a selected pixel indicated in red.

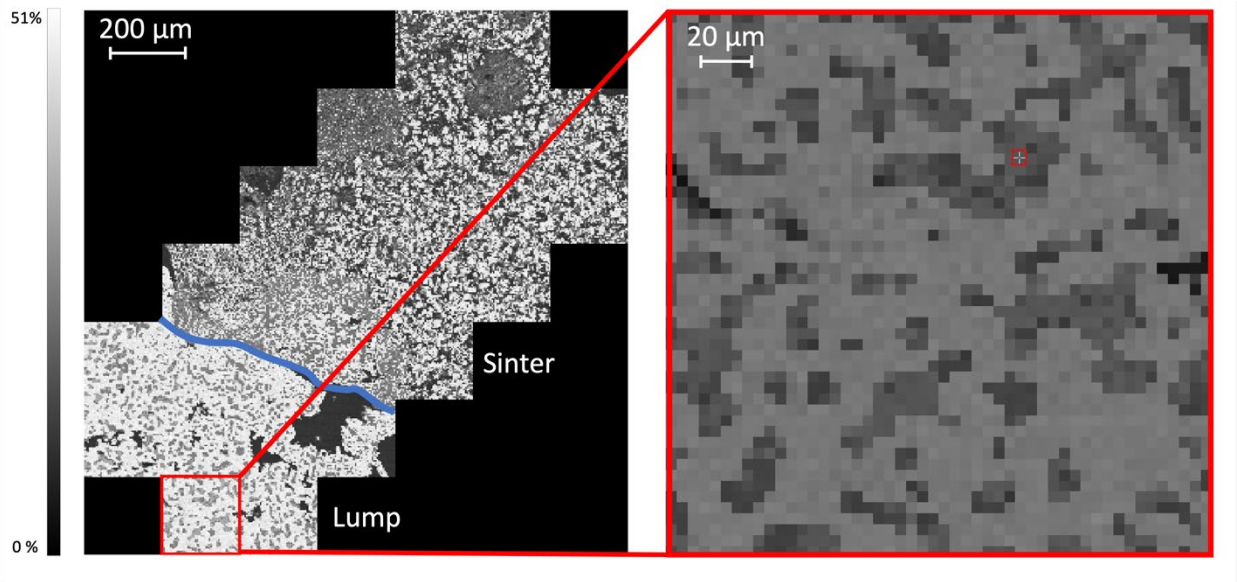

FIG 2 – BSE of scanned area for detailed analysis (left) and enlarged field (right). A single 4 µm pixel is outlined in red in the enlarged field (right). An approximate interface between the burdens is indicated by the freeform blue line (left).

Data Processing

Following the acquisition scan, Python 3.1 scripts were used to automate the retrieval of spectra from each pixel. The corresponding elemental composition of each 4 µm pixel was determined from the measured EDS spectra using the standardless quantification tool in the TIMA software (version 2.8.1). For standardless quantification, carbon was specified as the coating element, with the removal of escape peaks and sum peaks (spectral artefacts). Analysis was performed for Mg, Ca, Fe, Al, Si and O (all measured) and results returned as normalised atomic percent compositions.

The Python scripts output pixel coordinates and their associated compositions. The collected data was processed using a MATLAB script (2022b), from which the respective element maps were reassembled and an input file was generated for use in FactSage calculations. As only the properties of the oxide slag were to be calculated, pixels of metallic iron (determined as >80 at% Fe) were excluded from the FactSage input file.

Equilibrium Calculation

The generated input files from MATLAB were imported by a FactSage 8.2 Equilibrium Module macro (FToxid, FactPS). The macro sequentially performed equilibrium calculations for each pixel composition, writing results back to the input file. The input composition for the calculation was the quantified elemental composition as measured by EDS i.e. no assignment of stoichiometry was assumed. All solution and solid phases were selected, with duplicates suppressed (priority order FToxid > FactPS). The calculation temperature was set as 1300 °C (the experiment interruption

temperature). The key outputs from the equilibrium calculations were the amount of liquid slag and solid oxides, as well as their composition.

Image Reassembly and Presentation of Data

Results from FactSage calculations were imported back to MATLAB for reassembly into the final images. From the calculated quantities, properties such as the liquid fraction could be determined for each pixel by normalising to total oxide amount (i.e. excluding metallic iron). A summary of the above discussed workflow is shown in Figure 3.

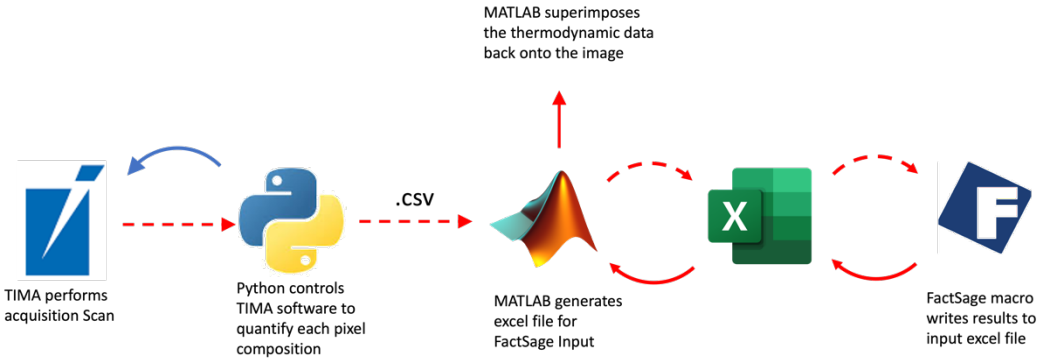

FIG 3 – Flow of information for developed workflow. Dotted red lines represent the flow of information leading up to the thermodynamic calculation, while solid red lines represent the processing of data into an image.

In addition to presenting calculated thermodynamic properties directly on the original microstructure, the data obtained during calculation can be presented in many formats to enhance interrogation of the data. One such method is to average the calculated compositions in a particular direction, allowing the system to be represented in a one-dimensional line. Analysis in such manner allows expression of multiple data sets on a single graph.

In the context of the interface analysed in this study, the compositions were averaged in the direction normal to the interface, so as to provide a one-dimensional representation of composition changes across the interface. To provide additional context to the determined properties, the averaged composition was inclusive of metallic iron, and also demonstrates the change in liquid composition with distance from the interface.

RESULTS

To demonstrate the developed technique, calculated properties are presented for the interface of lump and sinter shown in Figures 1 and 2. The quantified element maps are first shown to provide context for the proceeding calculated properties. Following the element maps, the calculated liquid fraction is shown alongside the solid phase stability maps. Finally, the average line compositions across the interface are shown.

Element Maps

The individual element maps as determined by standardless quantified SEM-EDS spectra (30,000 x-ray counts) is shown in Figure 4. Note that iron (Fe) and oxygen (O) are presented on a scale of 0 – 100 atomic percent (at%), while gangue elements (Si, Ca, Al and Mg) are shown on a scale of 0 – 50 at% to allow for greater contrast. The dotted lines are included as a reference line for the averaged line compositions discussed later.

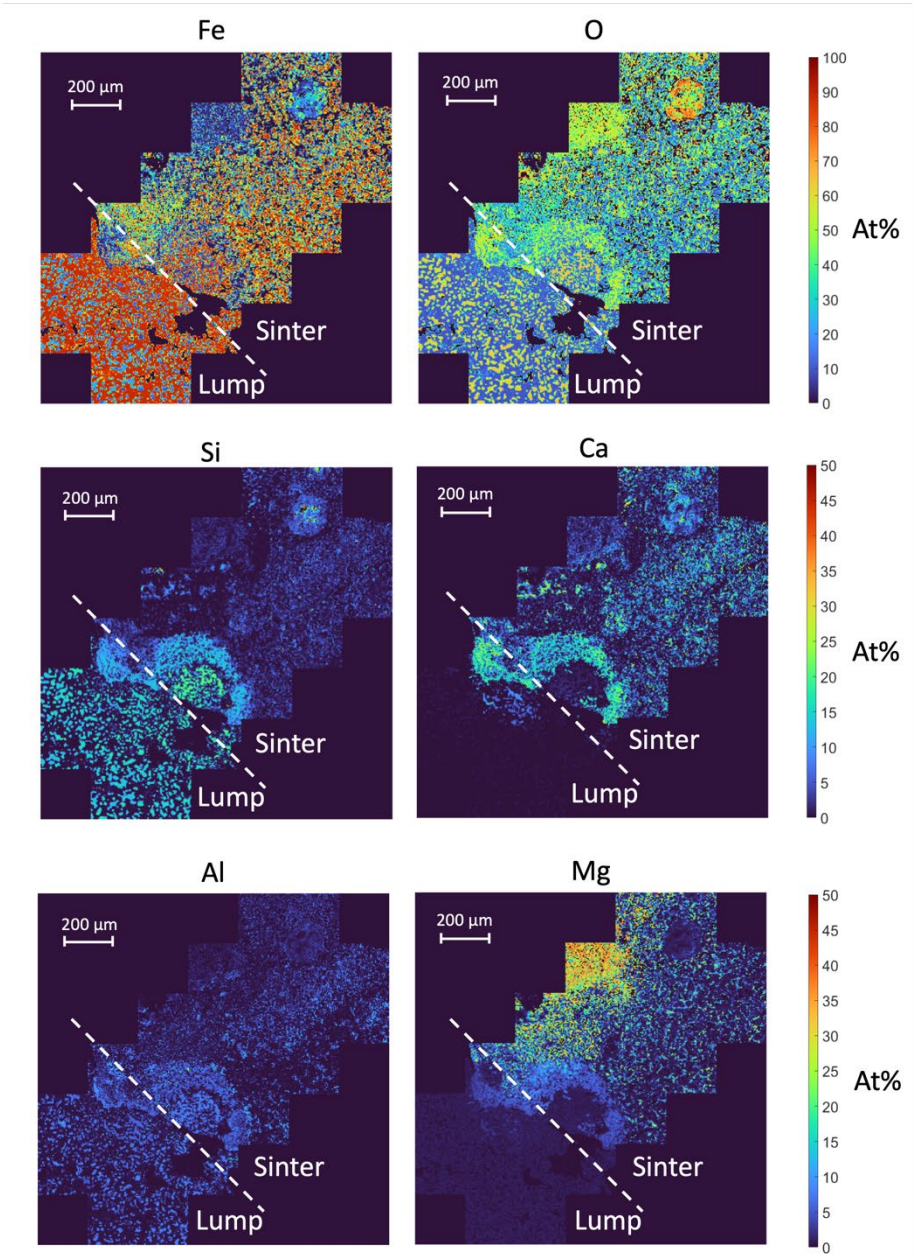

FIG 4 – Element maps as produced by standardless quantification of SEM-EDS spectra. Note that Fe and O are presented on a scale of 0 – 100 at%, while Si, Ca, Al and Mg are on a scale of 0 – 50 at%.

From Figure 4, the local variation in composition across the interface is evident. It is worth noting that the local composition can vary quite significantly from the bulk composition reported in Table 1. From the Fe map, metallic iron in the lump ore is seen to be an interconnected network. Additionally, the primary gangue in the lump ore is silicon based. Conversely, the sinter is observed to contain well distributed calcium, as well as a local region of magnesium. These local variations in composition provide key context to the proceeding calculations.

The most interesting variations in composition occur at the interface between the dissimilar burdens. The element maps indicate that a region of increased silicon occurs within the sinter close to the interface, with a curved region of accumulated calcium. The properties of this region are of key importance to the interpretation of the burden interaction mechanism.

Oxide Phase Stability

The dominant equilibrium phases that are predicted to have existed at 1300 °C, calculated from the compositions presented in Figure 4, are shown in Figure 5.

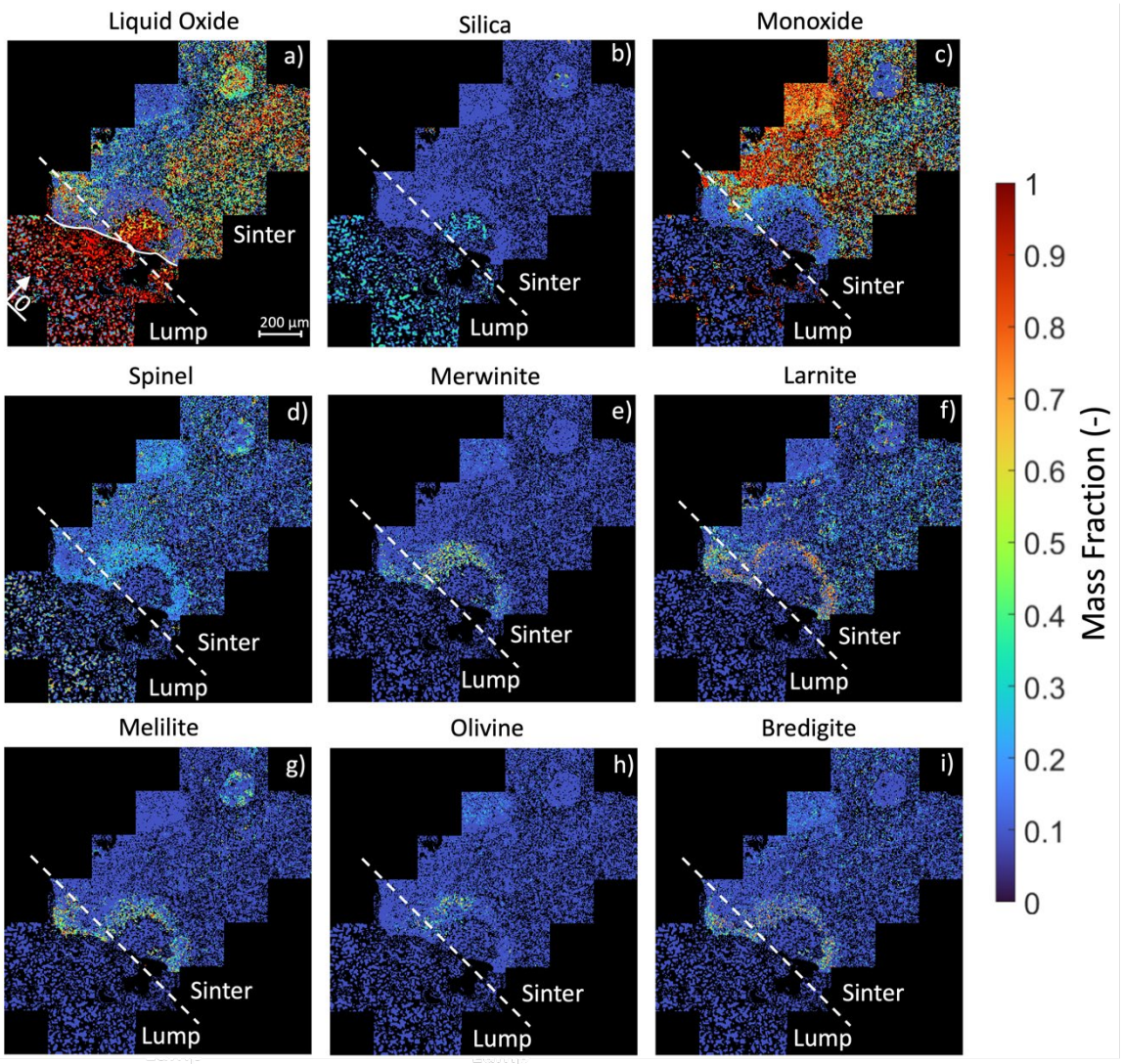

FIG 5 – Equilibrium phases determined by FactSage using composition input from element maps in Figure 4.

Figure 5 presents key insights into the spatial distribution of phases around the interface between the lump and sinter at 1300 °C. Additionally, mechanisms of interaction are evident through comparison of phases present in the bulk of the respective burdens and those at the interface. In the analysis of the predicted phases in Figure 5, it is assumed that no changes to the microstructure occurred on cooling.

From Figure 5(a), the lump ore is seen to contain a significant proportion of phases that would have been liquid at 1300 °C. The liquid phase is dispersed through the metallic iron network, with some remaining solid phases present. Through comparison with Figures 5(b) and 5(d), the solid phases remaining in the lump are primarily silica (SiO_2) and spinel ($FeAl_2O_4$). On the sinter side of the interface, the evenly distributed phases are partially molten (regions between 30-70 wt% liquid). A clear region with significantly lower liquid formation is seen in the upper left region of the sinter, directly correlating with the region containing magnesium in Figure 4. From Figure 5(c), the primary phase in this region is monoxide (MgO). In other regions of the sinter, the remaining solid phases are mostly larnite (Ca_2SiO_4) and spinel ($(Mg,Fe)Al_2O_4$).

At the interface between the two burden particles, a curved band of low liquid formation (Figure 5(a)) is seen, which directly corresponds to a region of unique mineral phases (Figure 5(e-i)). Specifically, where the oxide phases of the two burdens have interacted, merwinite ($Ca_3MgSi_2O_8$), melilite ($Ca_2(Mg,Fe)Si_2O_7$), olivine ($(Ca,Mg,Fe)_2SiO_4$) and bredigite ($Ca_7MgSi_4O_{16}$, $Ca_3Mg_5Si_4O_{16}$) are formed, as calculated by FactSage.

The mapping of properties through the developed technique is advantageous as it visually demonstrates the previously hypothesised interaction mechanisms reported in literature around a real ferrous burden interface.

Averaged Line Composition

Through comparison of all phase distributions presented in Figure 5, it can be observed that the interaction of the oxide phases between the burdens acts to suppress liquid formation through the stabilisation of new solid phases. In order to further elucidate the driving mechanisms of interaction, the liquid composition across the interface boundary is presented in Figure 6.

As previously discussed, Figure 6 presents the average composition across the interface between the burdens. The zero point of the imposed coordinates are marked at the bottom left of Figure 5(a), with the direction of averaging indicated by an arrow. As a reference point, the approximate location of the interface (marked by a dotted white line in Figures 4 and 5) is marked in Figure 6 as a dotted black line.

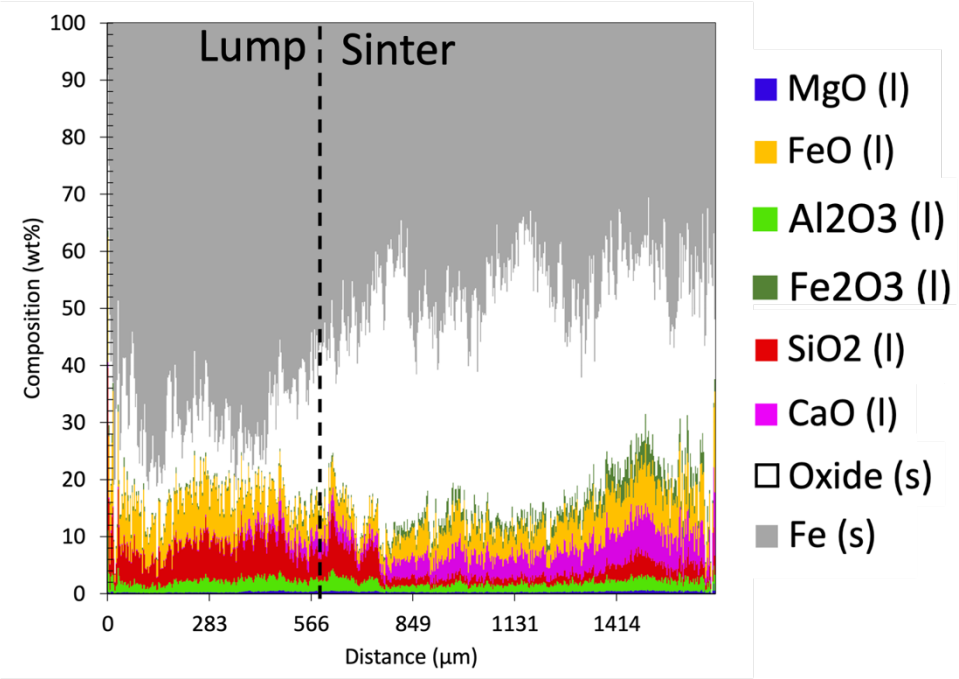

FIG 6 – Average line composition in direction normal to the interface between the burdens. Imposed coordinates are indicated at the bottom left of Figure 5(a).

In conjunction with Figures 4 and 5, the liquid composition in Figure 6 and the context of its surrounding microstructure (including the metallic iron presented in Figure 6) provide a holistic understanding of the interaction mechanisms occurring at the burden interface.

The lump liquids are primarily FeO/SiO_2 based (fayalitic), while the sinter liquids are dominated by $CaO/FeO/SiO_2$. An important insight from Figure 6 is that while the lump oxides have a higher fraction of liquids than the sinter (as also seen in Figure 5(a)), the oxide presence in the metallic structure is lower than that of sinter. This is in part due to the higher iron content of the lump (as seen in Table 1), as it does not contain additional oxide fluxes. Of note, MgO is not seen to participate significantly in the formed liquids at 1300 °C.

With an understanding of the composition of the formed liquids in the bulk materials, a mechanism of interaction can be directly observed, supporting previously proposed mechanisms (Liu, Honeyands, O'Dea, et al., 2019; Liu et al., 2014), and providing additional insight. Of particular importance, the dependency of liquid formation characteristics on the locally available oxides is evident.

These findings emphasise the importance of thermodynamic analysis using real, measured conditions from a particular heterogenous system. With the restricted intuition of pseudo-ternary phase diagrams in these systems, the technique presented in this study proves extremely useful in applying and understanding the appropriate thermodynamic analysis.

CONCLUSIONS

A novel data processing technique for overlaying calculated phase equilibria onto microstructures was developed. The integration of compositions determined by SEM-EDS element mapping with thermodynamic calculations provides an alternative visualisation tool for enhanced analysis while preserving spatial information. This technique is particularly advantageous in multi-component, heterogenous metallurgical systems, for which compositions cannot be expressed in a single pseudo-ternary diagram.

The newly developed technique was demonstrated through detailed analysis of the interface between a lump and sinter particle in a softening and melting test at 1300 °C. Mechanisms of interaction between the oxide phases of the dissimilar burdens were observed directly on the microstructure. Specifically, a region of suppressed liquid formation was seen, in which unique mineral phases (such as merwinite, melilite, olivine and bredigite) were stabilised.

The developed technique allows a visual application of the calculated thermodynamic properties, facilitating intuitive and automated interpretation of complex heterogenous microstructures. The further possibilities and applications of such an applied technique extend far beyond what is presented in this paper.

ACKNOWLEDGEMENTS

The authors gratefully acknowledge BHP for their financial support of the Centre for Ironmaking Materials Research, and permission to publish this work.

REFERENCES

Barrett, N., Mitra, S., Chew, S., O'dea, D., & Honeyands, T. (2023). Effect of Hydrogen Addition on Softening and Melting Performance of Lump and Sinter Mixed Burden. *ISIJ International, 63*(10), 1626-1636. doi:https://doi.org/10.2355/isijinternational.ISIJINT-2023-190

Barrett, N., Mitra, S., Copland, E., Chew, S., O'Dea, D., & Honeyands, T. (2024). Changes in Microscale Liquid Formation in Lump and Sinter Mixed Burden Softening and Melting Tests with the Addition of Hydrogen. *Metallurgical and Materials Transactions B*. doi:https://doi.org/10.1007/s11663-024-03062-w

Hoque, M. M., Doostmohammadi, H., Mitra, S., O'Dea, D., Liu, X., & Honeyands, T. (2021). High Temperature Softening and Melting Interactions Between Newman Blend Lump and Sinter. *ISIJ International, 61*(12), 2944-2952. doi:https://doi.org/10.2355/isijinternational.ISIJINT-2021-198

Kim, S.-H., Zhang, X., Ma, Y., Souza Filho, I. R., Schweinar, K., Angenendt, K., . . . Raabe, D. (2021). Influence of microstructure and atomic-scale chemistry on the direct reduction of iron ore with hydrogen at 700°C. *Acta Materialia, 212*, 116933. doi:https://doi.org/10.1016/j.actamat.2021.116933

Liu, X., Honeyands, T., Evans, G., Chen, J., & O'Dea, D. (2019). *Chemical interaction between basic sinter and Newman blend lump analogues*. Paper presented at the Iron Ore Conference, Perth.

Liu, X., Honeyands, T., Evans, G., O'Dea, D., & Ellis, B. (2018). *Interaction Between Lump Ore and Sinter Under Simulated Blast Furnace Conditions*. Paper presented at the 8th International Congress on Science and Technology of Ironmaking, Vienna.

Liu, X., Honeyands, T., O'Dea, D., Chen, J., & Qiu, G.-J. (2019). Interaction between sinter and lump during softening and melting process. *Iron and steel international, 54*, 19-26. doi:https://doi.org/10.13228/j.boyuan.issn0449-749x.20190094

Liu, X., Wu, S., Huang, W., Zhang, K., & Du, K. (2014). Influence of High Temperature Interaction between Sinter and Lump Ores on the Formation Behavior of Primary-slags in Blast Furnace. *ISIJ International, 54*(9), 2089-2096. doi:https://doi.org/10.2355/isijinternational.54.2089

Lu, Y., Wu, S., Du, B., & Zhou, H. (2020). Increasing the Softening as well as Melting Behaviors for Iron Ore Materials within the Blast Furnace Cohesive Zone through the High-temperature Interactivity. *ISIJ International, 60*(7), 1461-1468. doi:https://doi.org/10.2355/isijinternational.ISIJINT-2019-713

Lyu, B.-b., Wang, G., Yang, F., Zuo, H.-b., Xue, Q.-g., & Wang, J.-s. (2023). Softening and melting behaviors of ferrous burden in hydrogen-rich blast furnace cohesive zone. *Journal of Iron and Steel Research International*. doi:https://doi.org/10.1007/s42243-023-00951-3

Lyu, B.-b., Yang, F., Wang, G., Zuo, H., Xue, Q., & Wang, J. (2023, 2023//). *Effect of Hydrogen-Rich Atmosphere on Softening and Melting Behaviors of Ferrous Burden in Blast Furnace Cohesive Zone.* Paper presented at the Advances in Pyrometallurgy, Cham.

Ma, L., Zhang, J., Wang, Y., Lu, M., Cai, Q., Xu, C., . . . Liu, Z. (2022). Mixed burden softening-melting property optimization based on high-silica fluxed pellets. *Powder Technology, 412*, 117979. doi:https://doi.org/10.1016/j.powtec.2022.117979

Vemdrame Flores, I., Matos, O., Lima da Silva, A., & Covcevich Bagatini, M. (2021). Microstructure and Porosity Evolution During the Reduction, Softening and Melting of Iron-Bearing Materials. *Metallurgical and Materials Transactions B, 52*(3), 1716-1738. doi:https://doi.org/10.1007/s11663-021-02140-7

Wang, Y., Diao, J., Xie, B., Qi, C., & Du, P. (2022). Melting-Dropping Property of Blast Furnace Charge on the Basis of Its Slag Formation Behavior. *Metals, 12*(6), 987. doi:https://doi.org/10.3390/met12060987

World Steel Association. (2023). World Steel in Figures [Press release]. Retrieved from https://worldsteel.org/steel-topics/statistics/world-steel-in-figures-2023/

Wu, S., Han, H., Xu, H., Wang, H., & Liu, X. (2010). Increasing Lump Ores Proportion in Blast Furnace Based on the High-temperature Interactivity of Iron Bearing Materials. *ISIJ International, 50*. doi:https://doi.org/10.2355/isijinternational.50.686

Wu, S., Lu, Y., Hong, Z., & Zhou, H. (2020). Improving the Softening and Melting Properties of Ferrous Burden with High Al2O3 Content for Blast Furnace by Ore Blending. *ISIJ International, 60*(7), 1504-1511. doi:https://doi.org/10.2355/isijinternational.ISIJINT-2019-833

Wu, S., Su, B., Liu, X., & Kou, M. Y. (2018). Optimisation of the blast furnace burden based on its primary slag formation behaviour. *Ironmaking and Steelmaking, 45*(1), 50-57. doi:https://doi.org/10.1080/03019233.2016.1237073